

Maximization of net optical gain in silicon-waveguide Raman amplifiers

Ivan D. Rukhlenko^{1*}, Chethiya Dissanayake¹, Malin Premaratne¹,
and Govind P. Agrawal²

¹Department of Electrical and Computer Systems Engineering, Monash University,
Melbourne, VIC 3800, Australia

²Institute of Optics, University of Rochester, Rochester, NY 14627, USA

ivan.rukhlenko@eng.monash.edu.au

Abstract: We present a novel method for maximizing signal gain in continuously pumped silicon-waveguide Raman amplifiers made with silicon-on-insulator technology. Our method allows for pump-power depletion during Raman amplification and makes use of a variational technique. Its use leads to a system of four coupled nonlinear differential equations, whose numerical solution provides the optimal axial profile of the effective mode area along the waveguide length that maximizes the output signal power for a given amplifier length and a preset input (or output) cross-section area. In practice, the optimum profile can be realized by varying the cross-section area of a silicon waveguide along its length by tapering its width appropriately.

© 2009 Optical Society of America

OCIS codes: (250.4390) Nonlinear optics, integrated optics; (230.4320) Nonlinear optical devices; (230.4480) Optical amplifiers; (230.7370) Waveguides; (250.5960) Semiconductor lasers

References and links

1. R. Claps, D. Dimitropoulos, and B. Jalali, "Stimulated Raman scattering in silicon waveguides," *Electron. Lett.* **38**, 1352 (2002).
2. R. Claps, D. Dimitropoulos, V. Raghunathan, Y. Han, and B. Jalali, "Observation of stimulated Raman amplification in silicon waveguides," *Opt. Express* **11**, 1731 (2003).
3. B. Jalali, V. Raghunathan, D. Dimitropoulos, and O. Boyraz, "Raman-based silicon photonics," *IEEE J. Sel. Top. Quantum Electron.* **12**, 412 (2006).
4. C. Headley and G. P. Agrawal, Eds., *Raman Amplification in Fiber-Optic Communication Systems*, (Academic Press, San Diego, 2005).
5. G. P. Agrawal, *Nonlinear Fiber Optics*, (Academic, Boston, 2007).
6. Q. Lin, O. J. Painter, and G. P. Agrawal, "Nonlinear optical phenomena in silicon waveguides: Modeling and applications," *Opt. Express* **15**, 16604 (2007).
7. X. Chen, N. C. Panoiu, and R. M. Osgood, "Theory of Raman-mediated pulsed amplification in silicon-wire waveguides," *IEEE J. Quantum Electron.* **42**, 160 (2006).
8. M. Krause, H. Renner, and E. Brinkmeyer, "Analysis of Raman lasing characteristics in silicon-on-insulator waveguides," *Opt. Express* **12**, 5703–5710 (2004).
9. H. Renner, M. Krause, and E. Brinkmeyer, "Maximal gain and optimal taper design for Raman amplifiers in silicon-on-insulator waveguides," in *Integrated Photonics Research and Applications Topical Meetings (IPRA 2005)*, paper JWA3.
10. M. Krause, H. Renner, and E. Brinkmeyer, "Efficiency increase of silicon-on-insulator Raman lasers by reduction of free-carrier absorption in tapered waveguides," in *Conference on Lasers and Electro-Optics (CLEO 2005)*, paper CThB1.
11. M. Krause, H. Renner, and E. Brinkmeyer, "Efficient Raman lasing in tapered silicon waveguides," *Spectroscopy* **21**(1), 26–32 (2006).

12. D. Dimitropoulos, R. Jhaveri, R. Claps, J. C. S. Woo, and B. Jalali, "Lifetime of photogenerated carriers in silicon-on-insulator rib waveguides," *Appl. Phys. Lett.* **86**, 071115 (2005).
13. S. Fathpour, K. K. Tsia, and B. Jalali, "Energy harvesting in silicon Raman amplifiers," *Appl. Phys. Lett.* **89**, 061109 (2006).
14. A. Liu, H. Rong, M. Paniccia, O. Cohen, and D. Hak, "Net optical gain in a low loss silicon-on-insulator waveguide by stimulated Raman scattering," *Opt. Express* **12**, 4261 (2004).
15. R. Claps, V. Raghunathan, D. Dimitropoulos, and B. Jalali, "Influence of nonlinear absorption on Raman amplification in Silicon waveguides," *Opt. Express* **12**, 2774 (2004).
16. T. K. Liang and H. K. Tsang, "Role of free carriers from two-photon absorption in Raman amplification in silicon-on-insulator waveguides," *Appl. Phys. Lett.* **84**, 2745 (2004).
17. T. K. Liang and H. K. Tsang, "Nonlinear absorption and Raman scattering in silicon-on-insulator optical waveguides," *IEEE J. Sel. Top. Quantum Electron.* **10**, 1149 (2004).
18. I. D. Rukhlenko, M. Premaratne, C. Dissanayake, and G. P. Agrawal, "Nonlinear pulse evolution in silicon waveguides: An approximate analytic approach," *IEEE J. Lightwave Technol.* **28**, in press (2009).
19. I. D. Rukhlenko, M. Premaratne, C. Dissanayake, and G. P. Agrawal, "Continuous-wave Raman amplification in silicon waveguides: beyond the undepleted pump approximation," *Opt. Lett.* **34**, 536 (2009).
20. S. Roy, S. K. Bhadra, and G. P. Agrawal, "Raman amplification of optical pulses in silicon waveguides: effects of finite gain bandwidth, pulse width, and chirp," *J. Opt. Soc. Am. B* **26**, 17 (2009).
21. B. Jalali, O. Boyraz, V. Raghunathan, D. Dimitropoulos, and P. Koonath, "Silicon Raman amplifiers, lasers and their applications," in *Active and Passive Optical Components for WDM Communications V*, A. K. Dutta, Y. Ohishi, N. K. Dutta, and J. Moerk, eds., *Proc. SPIE* **6014**, 21-26 (2005).
22. C. Fox, *An Introduction to the Calculus of Variations* (Dover, New York, 1987).

1. Introduction

Owing to the perceived benefits of active silicon-photonics devices, there is a relentless interest in improving their performance since the first experimental demonstration of optical amplification via stimulated Raman scattering (SRS) in silicon-on-insulator (SOI) waveguides [1–3]. In addition to linear losses, which is the only inherent impairment in fiber optics [4, 5], silicon is plagued with two-photon absorption (TPA) and free-carrier absorption (FCA), two processes that dissipates energy of optical waves propagating through a silicon waveguide [6, 7]. To reduce the impact of TPA-induced FCA on Raman amplification, several theoretical and experimental studies have been carried out during the last five years [8–17]. Among others, several recently developed analytical and semi-analytical results, which provide a clear physical insight into the free-carrier effects in SOI waveguides deserve specific attention [18–20]. Particularly, an analytical solution describing propagation of single pulse through the SOI waveguides has been obtained in [18]. An approximate expressions for pump and signal intensities evolution along the single-pass silicon amplifier have been derived in [19]. In addition, the problem of continuous-wave (CW) Raman amplification of a signal pulse have been addressed semi-analytically using variational techniques in [20]. The results of these studies can be used to improve the performance of SOI-based Raman amplifiers. In this paper, we present another semi-analytical method that allows one to minimize the detrimental effects of FCA during the Raman amplification process.

The first and the most straightforward way to tackle the FCA problem involves decreasing the photogenerated carrier density inside the modal area by either decreasing the carrier lifetime [8, 15] or sweeping the carriers out of the waveguide by utilizing an external electric field [12, 13, 15, 21]. The other method of increasing the gain of a silicon Raman amplifier consists of adjusting the cross-section area of the SOI waveguide as well as its length appropriately [10]. Clearly, the optimal choice of these parameters is always possible because, for each fixed waveguide length, there is an optimal cross-section since zero cross-section corresponds to zero output signal power and an infinite cross-section implies absence of amplification. Similarly, for each fixed cross-section area, there is an optimal waveguide length since an infinite length corresponds to zero output signal power and a zero length implies absence of amplification. Hence, it should be possible to devise an algorithm that finds the optimal cross-section area and

optimal length of the SOI waveguide that maximize the signal gain for given input pump and signal powers.

Recently, waveguide tapering was suggested as an effective way to increase the efficiency of SOI-based Raman lasers [9–11]. The principle behind tapering consists of balancing of FCA and SRS processes inside the waveguide by varying its lateral dimensions. Numerical calculations have shown that width tapering allows one to significantly increase the output signal power in silicon Raman amplifiers, and reduce the lasing threshold of silicon Raman lasers, compared with the untapered situation [10, 11]. Under the undepleted pump approximation, the optimal tapering profile for CW silicon Raman amplifiers can be found analytically [9]. In fact, within this approximation, the optimal waveguide cross-section area as well as the pump and signal intensities have simple exponential forms along the amplifier length. However, even though the undepleted pump approximation can be justified for some Raman lasers, it is inapplicable in the case of Raman amplifiers, which ideally should be designed for total pump depletion and maximum signal amplification.

To the best of our knowledge, only a standard generic algorithm has been used up to now to find approximately the optimum axial profile of the effective mode area (EMA), related to the cross-section area of a SOI-based Raman laser [10]. This method cannot generate the exact optimal EMA axial profile along the waveguide length because it does not provide a systematic way to converge toward it. In this paper, we develop a novel numerical scheme, based on the variational principle, which allows one to find the exact EMA axial profile for a Raman amplifier that maximizes the output signal power. We reduce the optimization problem to a boundary-value problem for the pump and signal powers and two auxiliary functions introduced judiciously. Using our method for different lengths and input EMAs of a SOI waveguide, one can find the unique amplifier dimensions (cross-section area and length) that provide the maximum output signal power.

2. Variational approach and resulting equations

We focus on a silicon Raman amplifier that is pumped continuously at a frequency ω_p to amplify a CW signal at the frequency ω_s . Since optical phases do not play any important role during CW Raman amplification, we only need to consider the evolution of pump and signal powers (P_p and P_s) along the SOI waveguide. The two equations governing the SRS process in this situation are well known [6, 7] and can be written as:

$$\frac{dP_p}{dz} = -\alpha_p P_p - \beta_p \frac{P_p^2}{A_{\text{eff}}} - \zeta_{ps} \frac{P_p P_s}{A_{\text{eff}}} - \sigma_p \tau_c (\rho_p P_p^2 + \rho_s P_s^2 + \rho_{ps} P_p P_s) \frac{P_p}{A_{\text{eff}}^2}, \quad (1a)$$

$$\frac{dP_s}{dz} = -\alpha_s P_s - \beta_s \frac{P_s^2}{A_{\text{eff}}} - \zeta_{sp} \frac{P_s P_p}{A_{\text{eff}}} - \sigma_s \tau_c (\rho_p P_p^2 + \rho_s P_s^2 + \rho_{ps} P_p P_s) \frac{P_s}{A_{\text{eff}}^2}, \quad (1b)$$

where $\alpha_{p(s)}$ is the linear loss coefficient, $\beta_{p(s)}$ is the TPA coefficient, A_{eff} is the EMA of the propagating mode, β_{ps} is the cross-TPA coefficient, τ_c is the effective carrier lifetime, and ζ_{ps} and ζ_{sp} are the coefficients responsible for both cross-TPA and SRS:

$$\zeta_{ps} = 2\beta_{ps} + \frac{4g_R \gamma_R^2 \Omega_R \Omega_{ps}}{(\Omega_R^2 - \Omega_{ps}^2)^2 + 4\gamma_R^2 \Omega_{ps}^2}, \quad (2a)$$

$$\zeta_{sp} = \frac{\omega_s}{\omega_p} \left(2\beta_{ps} - \frac{4g_R \gamma_R^2 \Omega_R \Omega_{ps}}{(\Omega_R^2 - \Omega_{ps}^2)^2 + 4\gamma_R^2 \Omega_{ps}^2} \right). \quad (2b)$$

In these equations, $g_R = 76$ cm/GW is the Raman gain coefficient, $\Omega_R = 15.6$ THz is the Stokes shift, $\gamma_R = 105$ GHz is the Raman-gain bandwidth, and $\Omega_{ps} = \omega_p - \omega_s$. Finally, the FCA

effects are included in Eq. (1) through $\sigma_{p(s)} = \sigma_0(\lambda_{p(s)}/\lambda_0)^2$ with $\sigma_0 = 1.45 \times 10^{-21} \text{ m}^2$ and $\lambda_0 = 1550 \text{ nm}$. Also, $\rho_{p(s)} = \beta_{p(s)}/(2\hbar\omega_{p(s)})$ and $\rho_{ps} = 2\beta_{ps}/(\hbar\omega_p)$.

It follows from Eq. (1b) that, to maximize the net gain of signal at the end of the waveguide, we should maximize the functional

$$G(A_{\text{eff}}) = \int_0^L \frac{1}{P_s} \frac{dP_s}{dz} dz = \int_0^L g(z, A_{\text{eff}}) dz,$$

where L is the amplifier length and the local gain coefficient $g(z, A_{\text{eff}})$ is given by

$$g(z, A_{\text{eff}}) = -\alpha_s - \beta_s \frac{P_s(z)}{A_{\text{eff}}(z)} - \zeta_{sp} \frac{P_p(z)}{A_{\text{eff}}(z)} - \sigma_s \tau_c \frac{\rho_p P_p^2(z) + \rho_s P_s^2(z) + \rho_{ps} P_p(z) P_s(z)}{A_{\text{eff}}^2(z)}.$$

In contrast to the case of undepleted pump approximation, such a maximization does not require the local $g(z, A_{\text{eff}})$ to be maximum at each point z along the amplifier. This behavior results from a sophisticated differential relation between functions $P_p(z)$ and $P_s(z)$ which is clearly absent in the case of undepleted pump approximation.

We can solve the maximization problem using the standard method of the calculus of variations [22]. Let us assume that $A_{\text{eff}}(z)$ is the EMA axial profile for which G is stationary. Equating the variation δG to zero with respect to three variables, P_p , P_s , and A_{eff} , we obtain the relation

$$\int_0^L (\mathcal{A} \delta P_p + \mathcal{B} \delta P_s) dz = \int_0^L \mathcal{C} \delta A_{\text{eff}} dz, \quad (3)$$

where δP_p , δP_s , and δA_{eff} represent small axial variations in the three quantities and we have introduced

$$\begin{aligned} \mathcal{A} &= \frac{1}{A_{\text{eff}}} \left(\zeta_{sp} + \sigma_s \tau_c \frac{2\rho_p P_p + \rho_{ps} P_s}{A_{\text{eff}}} \right), \\ \mathcal{B} &= \frac{1}{A_{\text{eff}}} \left(\beta_s + \sigma_s \tau_c \frac{2\rho_s P_s + \rho_{ps} P_p}{A_{\text{eff}}} \right), \\ \mathcal{C} &= \frac{\beta_s P_s + \zeta_{sp} P_p}{A_{\text{eff}}^2} + 2\sigma_s \tau_c \frac{\rho_p P_p^2 + \rho_s P_s^2 + \rho_{ps} P_p P_s}{A_{\text{eff}}^3}. \end{aligned}$$

To find the connection between δP_p , δP_s , and δA_{eff} , we vary P_p and P_s in Eqs. (1) by small amount around fixed values and obtain

$$\frac{d(\delta P_p)}{dz} = -a_p \delta P_p - b_s \delta P_s + c_p \delta A_{\text{eff}}, \quad (4a)$$

$$\frac{d(\delta P_s)}{dz} = -a_s \delta P_s - b_p \delta P_p + c_s \delta A_{\text{eff}}, \quad (4b)$$

where

$$\begin{aligned} a_p &= \alpha_p + 2\beta_p \frac{P_p}{A_{\text{eff}}} + \zeta_{ps} \frac{P_s}{A_{\text{eff}}} + \sigma_p \tau_c \frac{3\rho_p P_p^2 + \rho_s P_s^2 + 2\rho_{ps} P_p P_s}{A_{\text{eff}}^2}, \\ b_p &= \mathcal{A} P_s, \quad c_p = \mathcal{C} P_p. \end{aligned}$$

The coefficients a_s , b_s , and c_s are obtained from a_p , b_p , and c_p by interchanging subscripts $p \leftrightarrow s$ and assuming that $\rho_{sp} = \rho_{ps}$.

Since the variations δP_p and δP_s are nonlinearly related to the variation δA_{eff} , we cannot solve Eq. (3) directly. However, it is still possible to express the optimal EMA axial profile, $A_{\text{eff}}(z)$, in terms of the pump and signal powers. To do this, we introduce two auxiliary functions, $\varphi(z)$ and $\psi(z)$, whose functional form is yet to be determined. However, apart from the existence of the derivative of these functions, Eqs. (1) do not impose any additional constraints on these functions. In particular, we can choose their end-point values (i.e., boundary values at the end of the amplifier) freely. Later, we make a specific choice in such a way that subsequent algebraic calculations are simplified.

Multiplying Eq. (4a) by φ and Eq. (4b) by ψ and integrating the resulting equations with respect to z from 0 to L , we obtain the following two equations:

$$\int_0^L \varphi \frac{d(\delta P_p)}{dz} dz = \varphi \delta P_p \Big|_0^L - \int_0^L \varphi' \delta P_p dz = - \int_0^L \varphi (a_p \delta P_p + b_s \delta P_s - c_p \delta A_{\text{eff}}) dz,$$

$$\int_0^L \psi \frac{d(\delta P_s)}{dz} dz = \psi \delta P_s \Big|_0^L - \int_0^L \psi' \delta P_s dz = - \int_0^L \psi (a_s \delta P_s + b_p \delta P_p - c_s \delta A_{\text{eff}}) dz,$$

where $\varphi' = d\varphi/dz$ and $\psi' = d\psi/dz$.

We assume that the boundary conditions at the left end of the amplifier for the pump and the signal are fixed so that their variations are equal to zero, i.e., $\delta P_p(0) = \delta P_s(0) = 0$. Since we are looking for a variational solution that maximizes the signal power at the waveguide output (i.e., at the right end of the amplifier), $\delta P_s(L) = 0$ as well. Because of these constraints, we do not need to set the boundary values for the auxiliary function ψ . However, we can simplify the algebra considerably by forcing $\varphi(z)$ to be equal to zero at the right end of the waveguide, i.e., by choosing

$$\varphi(L) = 0. \quad (5)$$

With this choice, the preceding two equations reduce to

$$\int_0^L [(\varphi a_p - \varphi') \delta P_p + \varphi b_s \delta P_s] dz = \int_0^L \varphi c_p \delta A_{\text{eff}} dz,$$

$$\int_0^L [\psi b_p \delta P_p + (\psi a_s - \psi') \delta P_s] dz = \int_0^L \psi c_s \delta A_{\text{eff}} dz.$$

Adding these equations termwise, we finally obtain the relation

$$\int_0^L [(\varphi a_p + \psi b_p - \varphi') \delta P_p + (\psi a_s + \varphi b_s - \psi') \delta P_s] dz = \int_0^L (\varphi c_p + \psi c_s) \delta A_{\text{eff}} dz. \quad (6)$$

A comparison of Eqs. (3) and (6) shows that the optimal EMA of the SOI waveguide can be found from a simple relation

$$\varphi c_p + \psi c_s = \mathcal{C}, \quad (7)$$

if the two auxiliary functions satisfy the differential equations

$$\varphi' = a_p \varphi + b_p \psi - \mathcal{A}, \quad (8a)$$

$$\psi' = a_s \psi + b_s \varphi - \mathcal{B}. \quad (8b)$$

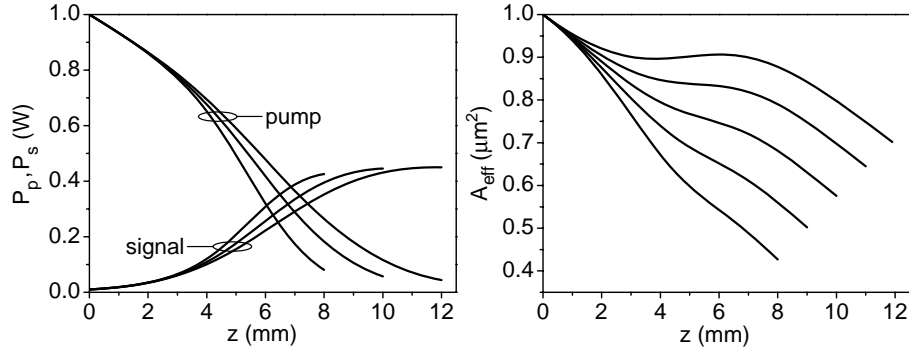


Fig. 1. Left panel: Evolution of the Pump and signal powers along SOI waveguides of three different length ($L = 8, 10, 12$ mm) with optimized EMA profiles. Right panel: Optimized EMA axial profiles for five waveguide lengths ranging from 8 to 12 mm. In all cases, $P_{p0} = 1$ W, $P_{s0} = 0.01$ W, and $A_0 = 1 \mu\text{m}^2$. See the text for other device parameters.

Equation (7) can be solved easily to provide the following relation:

$$A_{\text{eff}}(z) = \frac{2\tau_c [\sigma_s(1 - \psi P_s) - \sigma_p \varphi P_p] (\rho_p P_p^2 + \rho_s P_s^2 + \rho_{ps} P_p P_s)}{\varphi P_p (\beta_p P_p + \zeta_{ps} P_s) - (1 - \psi P_s) (\beta_s P_s + \zeta_{sp} P_p)}. \quad (9)$$

Irrespective of the input powers and waveguide parameters, this solution corresponds to the maximum of the functional G and thus maximizes net gain of the signal during Raman amplification. This can be proved by the following arguments. On the one hand, the output signal power, $P_s(L)$, equals to zero for all functions $A_{\text{eff}}(z)$ such that $A_{\text{eff}}(z_0) = 0$ for $z_0 < L$; by increasing the waveguide waist at $z = z_0$ from zero to some finite value, one can increase the output signal power. On the other hand, if for $z > 0$ the waveguide cross-section is so large that the nonlinear effects are negligible, $P_s(L)$ can be increased by narrowing the waveguide and enhancing the Raman amplification. Since the above analysis has revealed only one optimum $A_{\text{eff}}(z)$, we conclude that it should give a maximum value of G (otherwise there should be at least two other optimal functional forms of $A_{\text{eff}}(z)$ that correspond to the maxima of G).

Hence, our variational analysis shows that, to find the optimal EMA axial profile of the SOI waveguide (which is related to the optimum tapering of the waveguide width or cross-section area), we should solve the system of four coupled nonlinear differential equations, given in Eqs. (1) and (8), assuming that A_{eff} is given by (9). The 4 boundary conditions needed for solving these 4 equations come from the condition (5) and the three initial conditions: $P_p(0) = P_{p0}$, $P_s(0) = P_{s0}$, and $A_{\text{eff}}(z=0) = A_0$. The last condition can also be used at $z = L$ if the objective is to design a Raman amplifier with a preset EMA at the output end of the amplifier.

3. Numerical examples

We illustrate the versatility of our method by considering a silicon Raman amplifier with the following simulation parameters: $\lambda_p = 1550$ nm, $\lambda_s = 1686$ nm, $\alpha_p = \alpha_s = 1$ dB/cm, $\beta_p = \beta_s = \beta_{ps} = 0.5$ cm/GW, and $\tau_c = 1$ ns. Evolution of the pump and signal powers inside optimized amplifiers of three different lengths is shown in the left panel of Fig. 1. The right panel in the same figure shows the optimum EMA axial profiles for five amplifiers designed with $A_{\text{eff}} = 1 \mu\text{m}^2$ at $z = 0$. The incident pump and signals powers were assumed to be $P_{p0} = 1$ W and $P_{s0} = 0.01$ W. As mentioned earlier, the signal power is maximized at the output end of the amplifier rather than at each point along the waveguide. The longer the amplifier, the larger the output modal area and the smaller the tilt of the EMA axial profile needed for optimization.

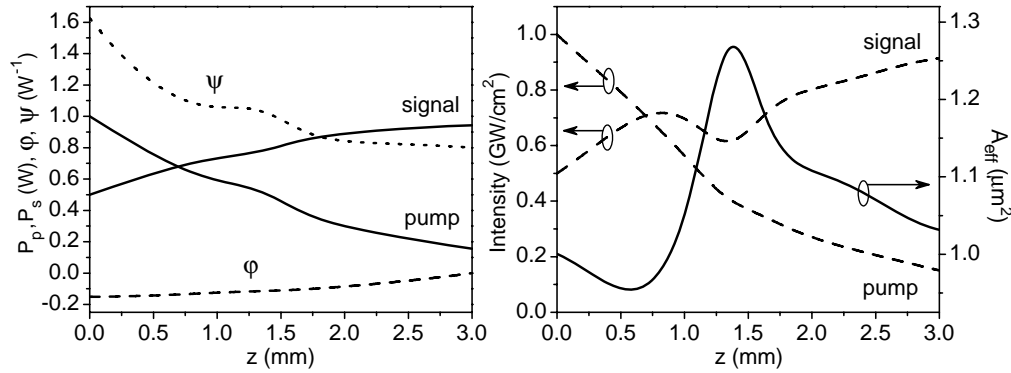


Fig. 2. Left panel: Solution of Eqs. (1) and (8) for a 3-mm-long waveguide with input values $P_{p0} = 1$ W, $P_{s0} = 0.5$ W, and $A_0 = 1 \mu\text{m}^2$. Solid curves show the pump and signal powers; dashed and dotted curves represent the two auxiliary functions. Right panel: Optimized EMA profile (solid curve, right scale) and the pump and signal intensities (dashed curves, left scale) corresponding to the pump and signal powers shown on the left panel.

This is because for longer amplifiers, Raman energy conversion should take place further from the input end to minimize losses. In fact, to provide such a delay in energy conversion, in some cases the modal area should even increase locally at a certain position of the waveguide. This feature is apparent in the right panel of Fig. 1 for the longest Raman amplifier for which the initially decreasing modal area increases slightly between 4 and 6 mm. Note also that the output signal power exceeds 0.4 W in all four cases, corresponding to a net gain by more than a factor of 400 in spite of the TPA and FCA. This is possible because our theory allows for significant pump depletion.

The extent of pump depletion is apparent in the left panel of Fig. 2 where we show the optimized solution in the case of a 3 mm-long amplifier by plotting variations along the amplifier length of the pump and signal powers together with those of the two auxiliary functions. Now the incident powers, $P_{p0} = 1$ W and $P_{s0} = 0.5$ W, are so high that the EMA of the silicon waveguide should even increase by about 30% between 0.6 and 1.4 mm (see the right panel in Fig. 2). In this case, the pump and signal intensities (dashed curves in the right panel of Fig. 2) decrease for a while, because it reduces the pump depletion (flattens the pump power profile) and thus conserves pump's power for subsequent energy conversion closer to the waveguide output. The main point to note is that, even in this highly saturated regime, pump is able to transfer about 85% of its power to the signal, in spite of losses resulting from TPA and FCA.

It is interesting to compare Raman amplification provided by optimized silicon waveguides with that occurring in the case of untapered as well as linearly tapered waveguides. Such a comparison is shown in Fig. 3. Solid curves represent the dependence of output signal power on the output EMA for four linearly tapered waveguides. The dotted line corresponds to the waveguide with a constant EMA of $1 \mu\text{m}^2$. The crosses represent the output signal powers realized with optimum tapering in the four cases displayed in Figs. 1 and 2. As one may expect, silicon waveguides with a constant EMA all along their length perform the worst in some cases. For example, the output signal power is only 35% of that realized with the optimum EMA profile for an untapered 8-mm-long amplifier. A smaller enhancement of the output signal power (around 10%) occurs for a 10-mm-long waveguide, and nearly no enhancement is found for 12-mm- and 3-mm waveguides. What is more important from a practical perspective is our observation that, for each optimized amplifier there exist a linearly tapered waveguide which gives nearly the same signal amplification (its parameters are determined by the maxima of

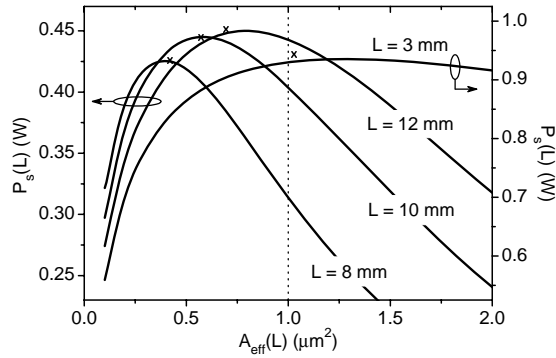


Fig. 3. Output signal power as a function of output EMA for linearly tapered waveguides of four different lengths. The incident powers correspond to those used in Figs. 1 and 2, and $A_0 = 1 \mu\text{m}^2$. The central dotted line represents a waveguide with constant EMA. The crosses show signal power and modal area at the end of the optimized waveguides in Figs. 1 and 2.

the solid curves). Thus, for example, instead of reproducing the modal area profile shown in the right panel of Fig. 2, one can reach the same signal gain by fabricating a linearly-tapered amplifier with the output EMA approximately equal to $1.3 \mu\text{m}^2$.

An important note concerning the applicability of the proposed method should be made. Clearly, the boundary-value problem that optimizes the amplifier “knows” nothing about the physical meaning of functions involved. As a result, physically meaningless solutions can sometimes arise in the case of very long amplifiers. These solutions lead to divergences in the EMA axial profile at some critical points z_i , where the denominator in Eq. (9) vanishes, and to negative values of A_{eff} between two successive critical points. Further work needs to be done to improve the stability of the numerical algorithm.

4. Conclusion

In conclusion, this paper has focused on the optimization of silicon Raman amplifiers in the saturation regime in which a substantial amount of pump power is transferred to the signal. We presented a novel numerical method for calculating the optimum EMA axial profile that provides the largest signal gain for a given value of the EMA and pump and signal powers at the input end of the amplifier. The implementation of the method requires numerical solution of a system of nonlinear differential equations, which contains twice as many equations as the original system describing the Raman amplification in a constant cross-section waveguide. We have solved these equations in several cases of practical interest and have found the optimum EMA profile that can be realized in practice by tapering the width of an SOI waveguide appropriately. We have also shown that in some cases the same maximal signal gain can be achieved by a simple linear tapering of the SOI waveguide. Our method is also applicable to the optimization of silicon Raman lasers with its suitable extension.

Acknowledgment

This work was funded by the Australian Research Council through its Discovery Grant scheme under grant DP0877232. The work of GPA is also supported by the NSF award ECCS-0801772.